University of Wales Trinity Saint David

Wales Institute of Science & Art



Application of

Computer Aided Engineering Processes

Structural Design & Fluid Analysis ACHA6010

Callum Carter-Davies

Student ID: 2008376

Date: 12/2023

Contents

1 Introduction 4

2 Literature Review 5

3 Validation 6

3.1 Deflection Under Load 6

3.2 Thermal Expansion 8

4 CAD Modelling and Assembly 11

5 Simulation and Analysis 12

5.1 Kinematics Study 12

5.2 Steady-State Thermal Study 13

5.3 Static Structural Study 14

5.4 Topology Study 17

6 Conclusions 21

7 References 22

Table 1 - Material properties used in the studies (ANSYS, 2021b). 12

Table 2 – Thermal study temperature data (Noble, n.d.) 14

Figure 1 - Deformation results for the static structural study. 6

Figure 2 - Effect of mesh size on deflection in CAD. 7

Figure 3 - Deflection with selection of boundary conditions 8

Figure 4 - Bimetallic strip deflection in ANSYS 8

Figure 5 - Simulated deformation due to thermal loading across a range of mesh sizes. 9

Figure 6 - Engine assembly in SOLIDWORKS 2023 11

Figure 7 - Connecting Rod model in SOLIDWORKS 2023 11

Figure 8 - Linked systems in ANSYS Workbench 12

Figure 9 - The direction of the force acting on the top end of the connecting rod at TDC. 13

Figure 10 - Thermal study results 14

Figure 11 - Forces acting on the connecting rod. 15

Figure 12 - Deformation of connecting rod in static structural study. 16

Figure 13 - von-Mises stress across the connecting rod 17
Figure 14 - The inertial forces acting on the simplified connecting rod. 18
Figure 15 - von-Mises stress results of the simple connecting rod. 18
Figure 16 - Deformation results of the simple connecting rod. 19
Figure 17 - Topology iterations 20

1 Introduction

Finite element analysis (FEA) was utilised to perform studies on a model of a connecting rod to identify areas where alterations to the geometry could be implemented. Simple models were solved analytically and through the use of FEA to verify the accuracy of the results of the studies. This also allowed for actions or boundary conditions, which are constraints applied to the structure, that may cause errors to be identified and avoided in studies to prevent misleading and inaccurate results. Topology optimisation was also used to identify inefficient parts of the connecting rod geometry that could be removed to reduce mass.

2 Literature Review

Computer Aided Engineering (CAE) programs perform FEA on a structure. FEA is used to simulate the effect of loads on a structure, allowing for an estimation to be made on the deformation and stresses occurring within the structure under specified conditions (Baccouch, 2021).

Discretisation is used to create a mesh representing the original model by dividing the structure of the model up into smaller elements, which approximate the shape of the original model(Hearn, 1997). Elements can be 1, 2, or 3 dimensional with each element being made up of nodes which define its degrees of freedom. 3D elements are typically hexahedral or tetrahedral (Rugarli & Rugarli, 2010). Discretisation does not completely replicate the shape of the object meaning there will always be errors in the results. As computers function is base 2 there are also errors in the results due to floating-point rounding errors (Goldberg, 1991).

The results of FEA can be used in determining the life cycle of the component based on fatigue. Areas of a material with high stress concentration being cyclically loaded can form cracks at points with defects, which propagate with further cyclic loading leading to material weakening and potentially failure. Fatigue testing can be performed on materials to create an S/N curve to approximate the life span of a component operating under certain conditions (Hearn, 1997). The roughness of the surface finish of the material affects the fatigue behaviour (Hidalgo et al., 2018).

3 Validation

A validation of the FEA method was performed to compare the results found through simulation against those calculated analytically. This would give an indication of the accuracy of the values produced by the FEA model.

3.1 Deflection Under Load

The deflection of a material under load was calculated analytically and modelled in CAD software to verify the accuracy of the CAD model. A cantilever beam model was used with 1 end fixed and a universally distributed load (*p*)of 2750 N/m^2 was applied across the top face of the material. The material used in this study was a structural steel with an elastic modulus (*E*) of 210 GPa. The beam had a length (*L*) of 1 m, width (*w*) of 0.05 m, and a thickness (*t*) of 0.005 m. The calculation used to determine the maximum deflection (U_{max}) is as follows:

$$U_{max} = \frac{3pL^4}{2Ew^2t}$$

After inputting the values:

$$U_{max} = \frac{3 * 2750 * 1^4}{2 * 210 * 10^9 * 0.05^2 * 0.005} = 0.01571 \text{ m}$$

The study was run using a 2.5 mm square mesh with the face on the end of the beam fixed. The maximum deflection was found to be 0.016394 m (Figure 1). The result from the CAD study was 4.35% more than the deflection calculated analytically, suggesting there were potentially rounding errors occurring in the calculation.

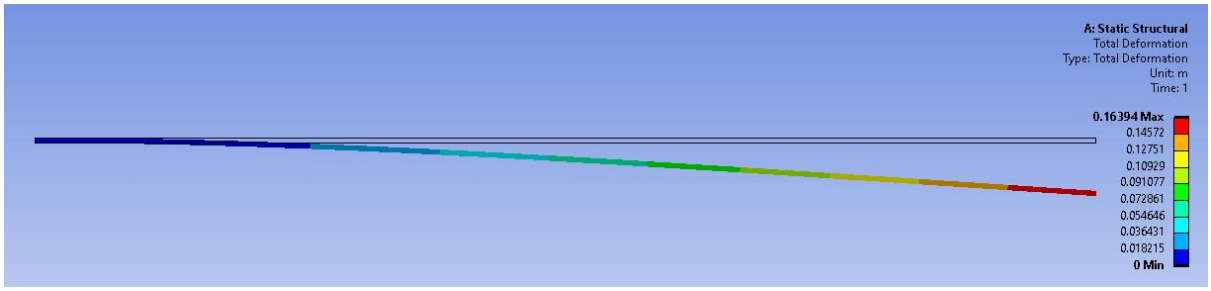


Figure 1 - Deformation results for the static structural study.

As the size of the mesh would affect the number of rounding errors occurring, the study was repeated across a range of mesh sizes. The mesh size was increased up to 35 mm until the study failed due to there not being enough elements to conduct it. The mesh size was also decreased down to a minimum of 0.5 mm, the software crashed at mesh sizes below this so it was not possible to reach a point of mesh independence.

The results of these studies (Figure 2) show as the mesh size decreases, there is a reduction in the deflection which suggests the presence of floating-point rounding errors.

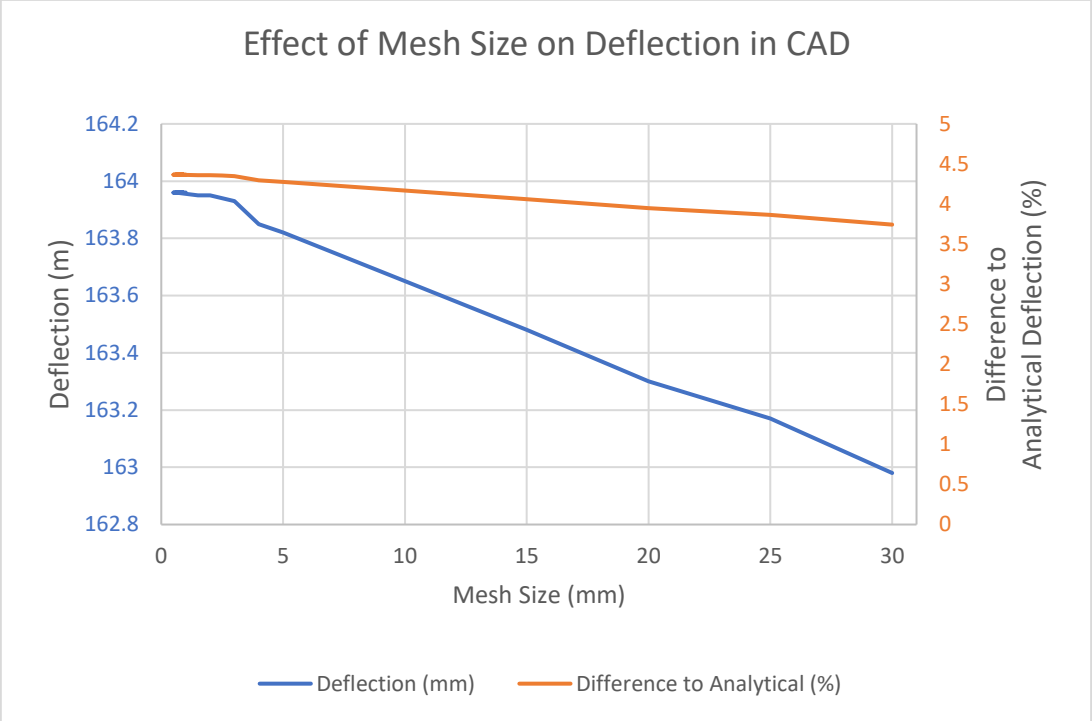


Figure 2 - Effect of mesh size on deflection in CAD.

It was considered that the parts of the geometry that were fixed may affect the results therefore several tests were run with the fixed portion being different parts of the geometry (Figure 3). These tests showed the fixed connection on the end face of the beam produced the result closest to the one found by the analytical method. In terms of setting boundary conditions, there was little difference between fixing the top and bottom edges compared to fixing all 4 edges, whereas the result for only fixing the side edges was extreme with a result 56% higher than the other methods of constraint. It's likely that the result for top and bottom would also be extreme if the force wasn't acting directly perpendicular to these edges. This shows that the constraints must be correctly established to avoid erroneous results.

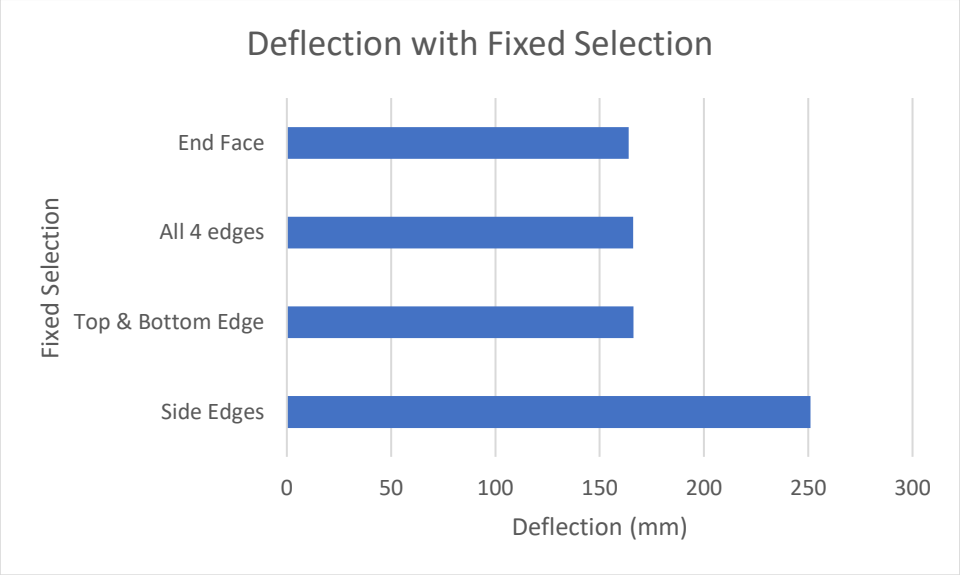


Figure 3 - Deflection with selection of boundary conditions

3.2 Thermal Expansion

The second validation case performed was investigating the simulation accuracy of the heating of a bimetallic strip (Figure 4). A bimetallic strip has 2 different metals joined together, as they are heated the difference between their coefficient of thermal expansion (CTE) causes a deflection to occur (Dlubal Software, 2017). The magnitude of the deflection is dependent on the geometry of the strip and the Modulus of Elasticity (E) of each material.

Copper has a CTE_c of 2×10^{-5} °C^{-1} and E_c of 130 GPa, and Invar has a CTE_i of 1.2×10^{-6} and E_i of 137 GPa. Both strips had length L of 100 mm, width w of 5 mm, and a thickness t of 1 mm. The strips were assumed to be bonded uniformly and were fixed by the face of the component at 1 end. The deflection was measured following the heating of the strips from an ambient temperature of 22 °C to a temperature of 122 °C, giving a thermal load T of 100 °C.

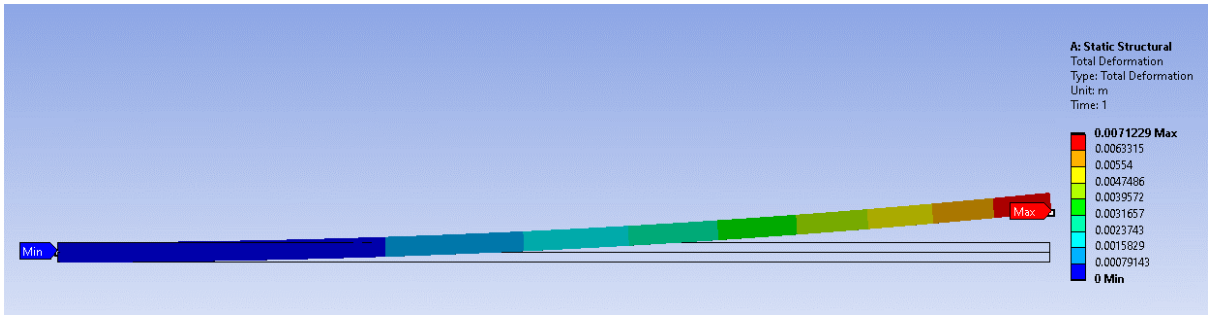


Figure 4 - Bimetallic strip deflection in ANSYS

For comparison against the simulation, the expected deflection U_{max} was calculated analytically, K_1 is a dimensionless coefficient used to determine a stiffness for the strip based on the *E* and *t* of the 2 materials:

$$K_1 = 4 + 6\frac{t_c}{t_i} + 4\left(\frac{t_c}{t_i}\right)^2 + \frac{E_c}{E_i}\left(\frac{t_c}{t_i}\right)^3 + \frac{E_i t_i}{E_c t_c}$$

$$K_1 = 4 + 6\frac{0.001}{0.001} + 4\left(\frac{0.001}{0.001}\right)^2 + \frac{130 \times 10^9}{137 \times 10^9}\left(\frac{0.001}{0.001}\right)^3 + \frac{137 \times 10^9 \times 0.001}{130 \times 10^9 \times 0.001}$$

$$K_1 = 16.003$$

$$U_{max} = \frac{6 \times (CTE_i - CTE_c) \times (t_i + t_c) \times T}{(t_c)^2 \times K_1} \times \frac{L^2}{2}$$

$$U_{max} = \frac{6 \times ((1.2 \times 10^{-6}) - (2 \times 10^{-5})) \times (0.001 + 0.001) \times 100}{(0.001)^2 \times 16.003} \times \frac{100^2}{2}$$

$$U_{max} = -0.007049\, m$$

The analytical method gave a value of 7.049 mm for the deflection of the strip under these conditions. The test was performed with mesh sizes of 0.1 mm up to 3.45 mm.

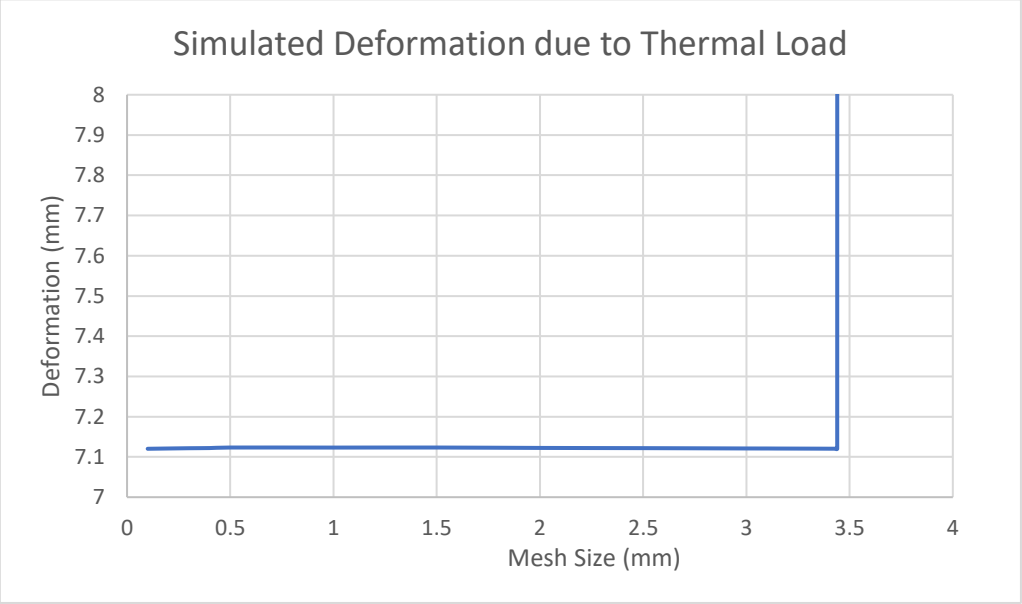


Figure 5 - Simulated deformation due to thermal loading across a range of mesh sizes.

As seen in Figure 5, the maximum deformation is approximately 7.121 mm, a 1.01 % increase over the deformation calculated analytically. Mesh independence was established at a mesh size of 3.44 mm. It is unknown how this error in deformation in both cases will be affected by a more complex geometry and loading case.

4 CAD Modelling and Assembly

The assembly used for the study (Figure 6) was part of a 1.6 L inline 4-cylinder engine modelled and assembled in SOLIDWORKS 2023 (2023) consisting of a piston, gudgeon pin, connecting rod, crankshaft, flywheel, and crankcase. The study focused on the connecting rod specifically (Figure 7) with some assumptions were made regarding its construction to simplify the process and avoid possible issues arising during studies. The bolts which are typically used to affix the 2 parts of the connecting rod that are typically bolted together were assumed to be 1 single piece. The bearings were not modelled and the contact between surfaces was assumed to be frictionless. The oil passages were not modelled.

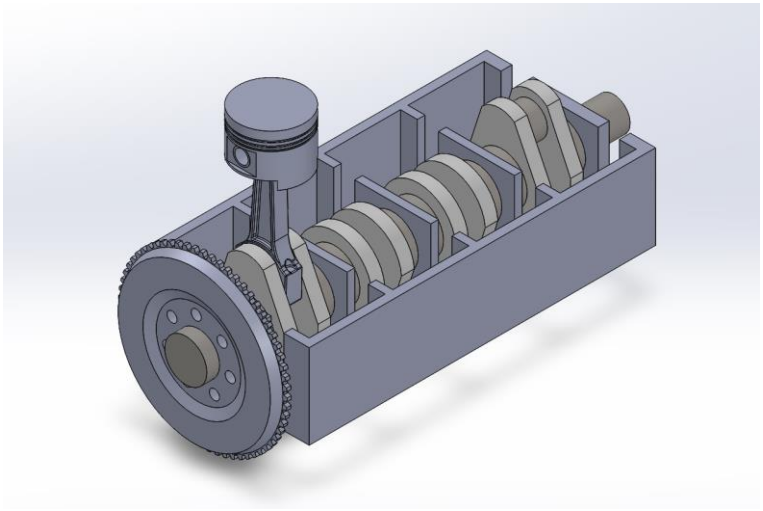


Figure 6 - Engine assembly in SOLIDWORKS 2023

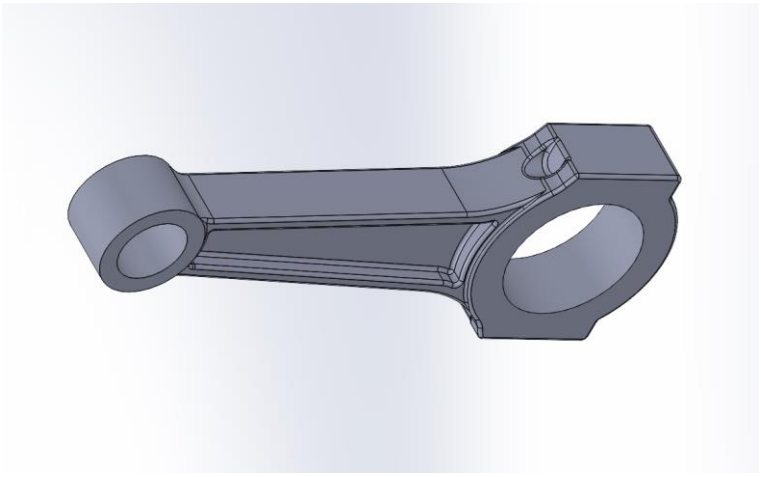


Figure 7 - Connecting Rod model in SOLIDWORKS 2023

5 Simulation and Analysis

To determine the performance of the piston under expected loads a 3-stage process was implemented (Figure 8) in ANSYS Workbench (2021). The first stage was a rigid body kinematics study used to determine the forces acting at various points throughout the assembly. Next, a thermal study was carried out to calculate the temperature throughout the material as this would influence the size and strength of the component. Finally, a static structural study was used to determine the impact of the loads calculated in the first stage, as well as applying the expected load from the piston under combustion, on the structure of the component.

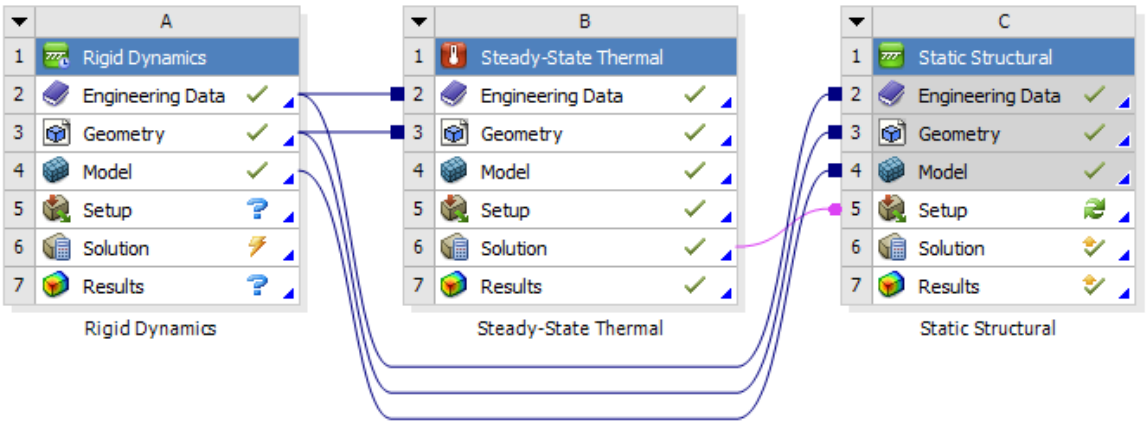


Figure 8 - Linked systems in ANSYS Workbench

The purpose of this was to determine stresses and deformation across the material and could be used to calculate the fatigue life for comparison against future iterations. The materials assigned to each component are detailed in Table 1, the material properties were sourced from Granta EduPack (2021).

Table 1 - Material properties used in the studies (ANSYS, 2021b).

Material	**Density (kg/m^3)**	**Young's Modulus (MPa)**	**Ultimate Tensile Strength (MPa)**	**Ultimate Yield Strength (MPa)**
T6 Aluminium Alloy	2.713	69040	313.4	259.2
Structural Steel	7.85	20000	460	250

5.1 Kinematics Study

A kinematics study was conducted to determine the forces acting on each end of the connecting rod from the inertia of components during engine operation at 6000 rpm, rotated at the pulley end of

the crankshaft. For this study, all components were considered to be rigid and only the inertia loads were accounted for. The crankcase was fixed in place by the bottom face and the top face of the outer wall. The crown of the piston was restricted to only translate on the axis of reciprocation to simulate it being restricted by the cylinder walls however in reality it may have some rotation around the joint with the gudgeon pin.

A joint probe was utilised to record the force acting through the connection of the gudgeon pin and the upper end of the connecting rod. The largest forces were acting along the Y-axis of the connecting rod and ranged from 5176N at bottom dead centre (BDC) to -9331N at top dead centre (TDC) (Figure 9).

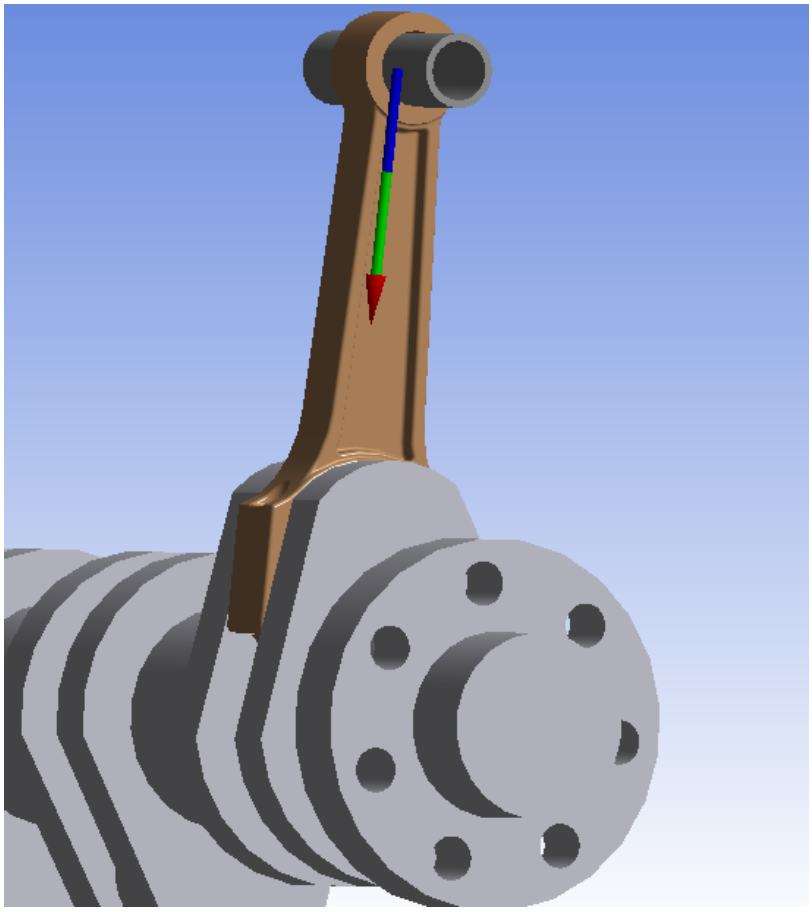


Figure 9 - The direction of the force acting on the top end of the connecting rod at TDC.

A study by Shenoy (2006) showed the resultant forces acting on a connecting rod peaked at around 13 kN at 5700 rpm, however this also took the force from combustion pressure into consideration.

5.2 Steady-State Thermal Study

The steady-state thermal analysis was used to consider the effect of heat on the material's ability to resist deformation. The thermal transfer was based on the heat transfer from the piston crown through the piston and the gudgeon pin.

The data used for the thermal study is shown in Table 2.

Table 2 – Thermal study temperature data (Noble, n.d.)

Part	Heat Transfer Coefficient	Temperature (°C)
Piston Crown Top	497.5	928.5
Piston Crown Side	447.5	425
Piston Top & Mid Groove	437.5	190
Piston Oil Groove	338.75	163.75
Piston Underside	462.5	91.25
Gudgeon Pin	338.75	163.75
Connecting Rod	300	91.25

The thermal study determined the temperature across the connecting rod to be in the range of 93 °C to 213 °C. This was higher than expected and could be due to the assumed heat transfer coefficient for the connecting rod or the gudgeon pin being incorrect as these were estimated due to not being able to find data for them.

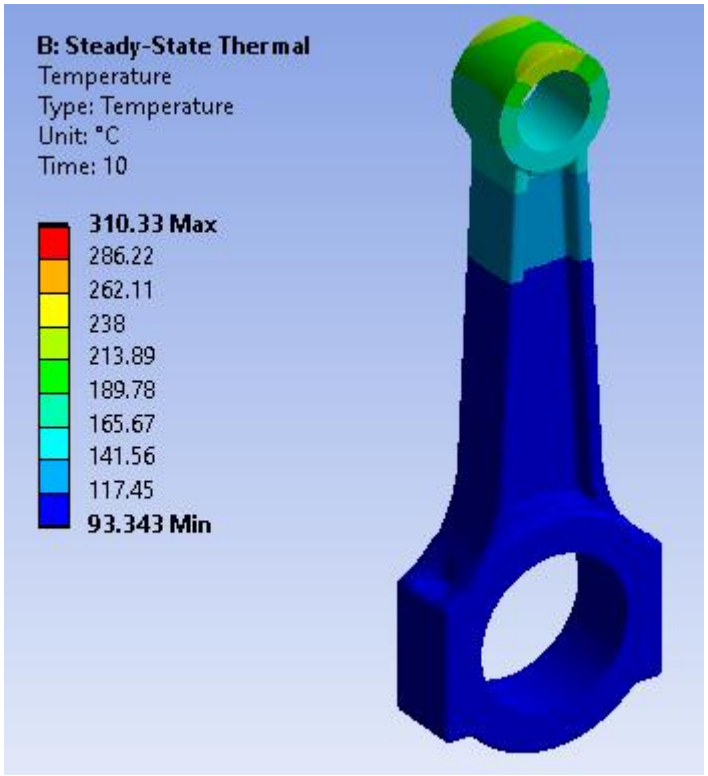


Figure 10 - Thermal study results

5.3 Static Structural Study

The von-Mises stress and deflection of the material was determined through a static structural study. This study combined the forces found in the kinematics study and the heat load estimated through the thermal study to approximate the stress and deflection of the connecting rod. A fixed

connection to ground was not used at this would prevent parts of the model from deforming, so weak springs were used to hold it in place instead. The maximum load from the kinematics study was used in this static structural test (Figure 11).

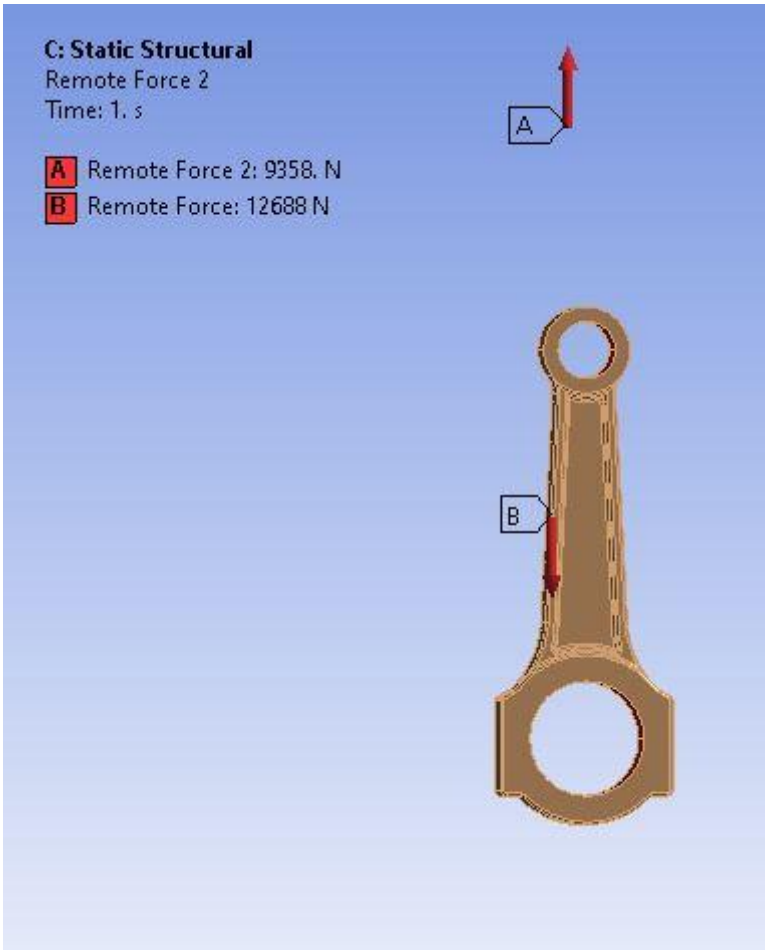


Figure 11 - Forces acting on the connecting rod.

The study found 1 side of the lower end of the connecting rod underwent the most deformation at 0.33 mm as well as a significant portion of the structure experiencing deformation of around 0.2 to 0.25 mm (Figure 12).

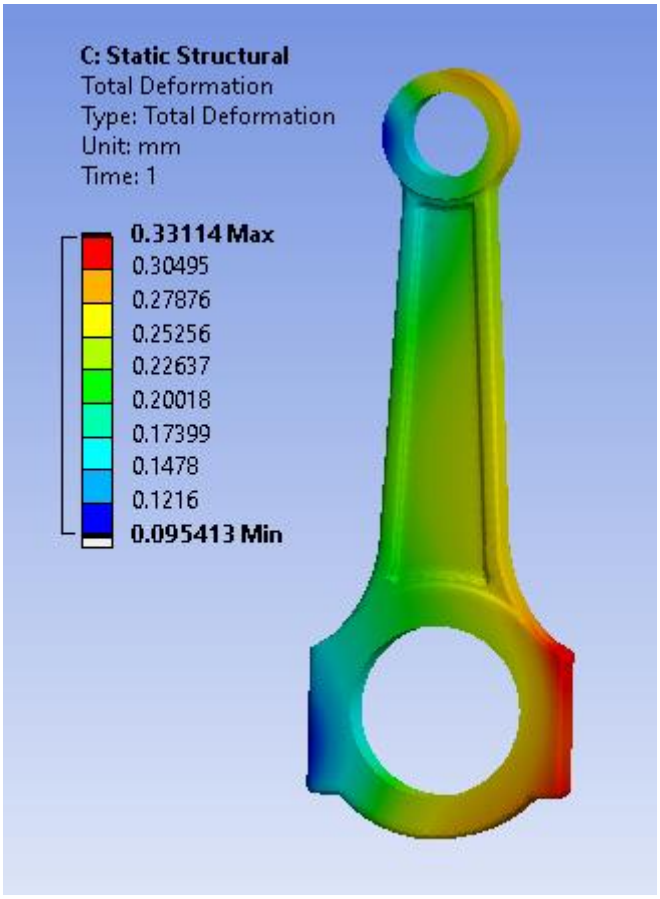


Figure 12 - Deformation of connecting rod in static structural study.

Most of the stress was concentrated on 1 side of the connecting rod, with the maximum stress occurring at the join between the beam and the upper end. The maximum stress value was determined to be 219 MPa, while this is under the ultimate yield strength of 259 MPa this would become more relevant over the life of the component as the connecting rod is subjected to repeated cyclic loading which would cause fatigue. The number of cycles the component would be expected to endure before failure would be dependent on the use case, in a

In a future iteration, the top of the beam could be wider to make a shallower angle between the beam and the upper end to spread out the stress concentration. There is also the potential that this stress concentration is due to error in how the stress was calculated due to the mesh density around the fillet however that isn't seen at the other fillet points.

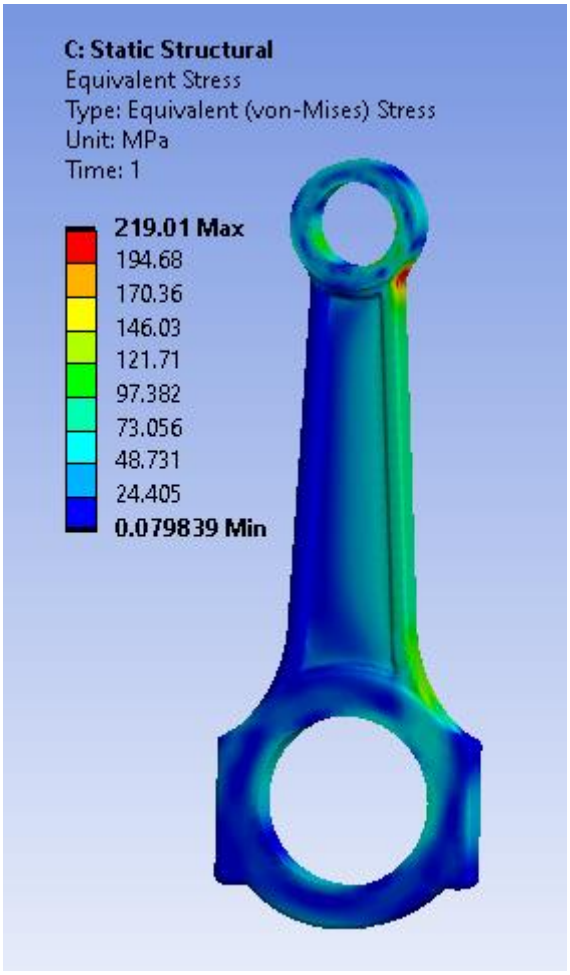


Figure 13 - von-Mises stress across the connecting rod

5.4 Topology Study

A topology study was run to optimise the mass of the connecting rod while having minimal impact on the strength of the component under the given loads. This allowed for the removal of unnecessary material in future iterations to make a closer representation of the optimal component shape for the use case. A simplified connecting rod shape was used as this would be less restrictive, allowing for more flexibility for material removal in the topology iterations.

The inner circumference of the top and bottom end of the connecting rod were required to be a specific shape and size so they were excluded from the study. The forces calculated during the kinematics study were larger than previously due to the extra mass of the simple connecting rod (Figure 14). The simple connecting rod underwent the same studies performed for the original connecting rod, which gave values for the von-Mises stress (Figure 15) and deformation of the component (Figure 16).

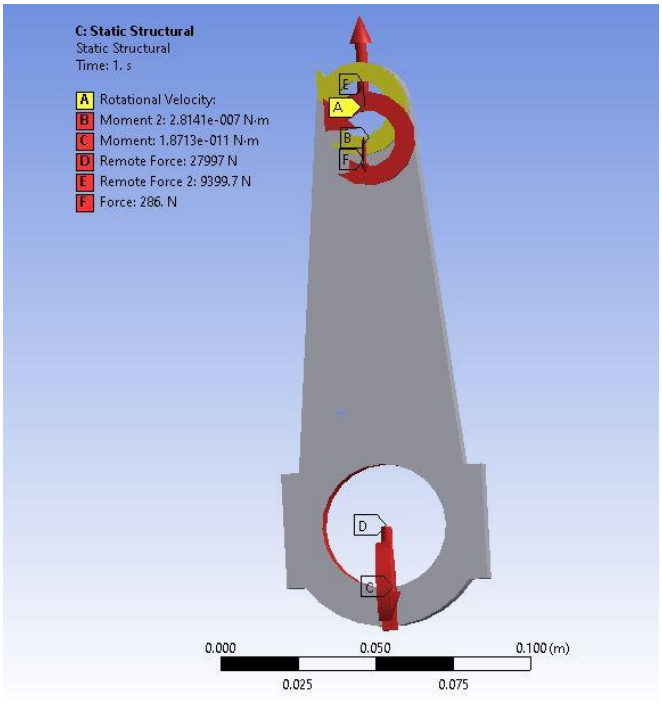


Figure 14 - The inertial forces acting on the simplified connecting rod.

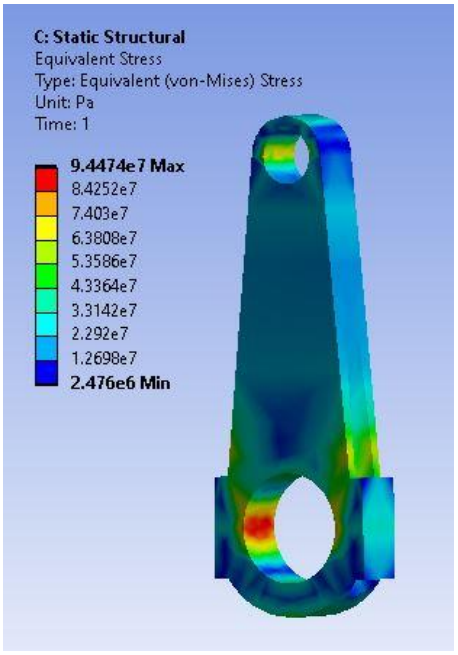


Figure 15 - von-Mises stress results of the simple connecting rod.

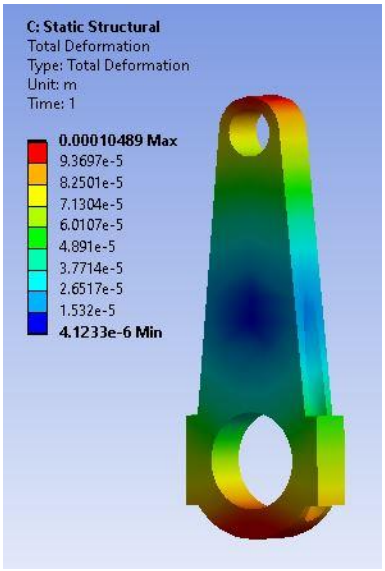


Figure 16 - Deformation results of the simple connecting rod.

There is a clear difference in the magnitude and locations of stress concentration between the simple connecting rod and the original connecting rod. Some of this difference is likely due to the difference in geometry, with the simple connecting rod not having the corner fillet towards the top of the beam. It appears the direction of the force is not consistent between the 2 studies.

The topology optimisation was performed with the objective of removing 30% of the mass whilst maintaining or reducing the von-Mises stress. This did not account for the change in inertial forces based on the mass difference. The topology study finished after 16 iterations (Figure 17) and showed the material in the centre of the connecting rod's beam was less efficient in terms of the amount of stress it can handle for its mass than the material on the outer edge, top, and base of the beam. The material shown in the 16th iteration is mainly around the places determined to have the most stress in the static structural study. The applied loads, targets, and objectives could be adjusted to try to refine the way the topology forms as the loading varies significantly throughout a cycle.

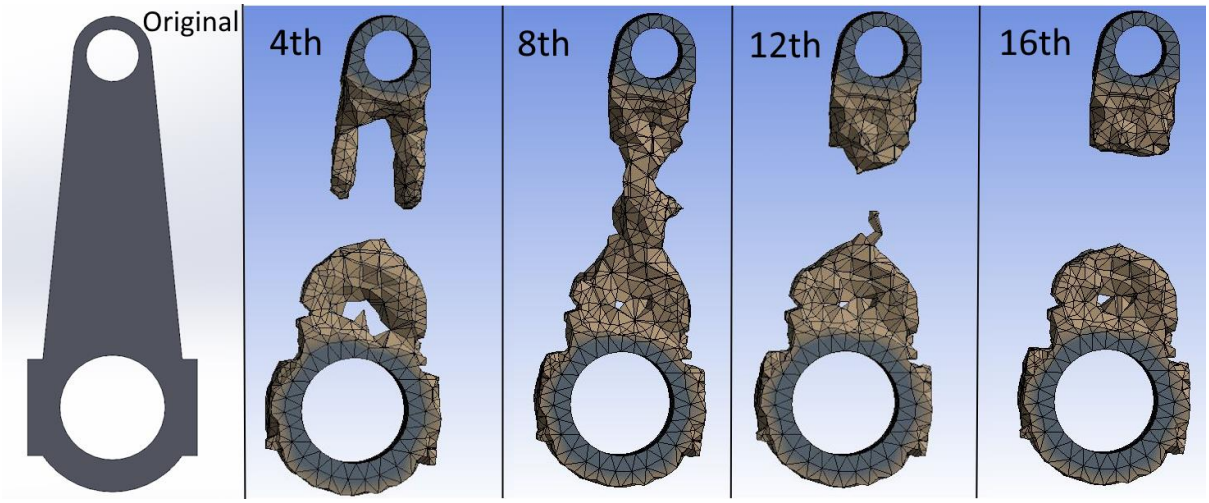


Figure 17 - Topology iterations

6 Conclusions

From the validation methods it was apparent that the FEA solver tended to slightly overestimate the impact of the load, by approximately 1% and 4% for the bimetallic strip and cantilever beam respectively. The way in which constraints were applied had a significant impact on the results of the study with variations of up to 56% given the same loads.

The stresses calculated through FEA were similar to those found from other studies however there were many variables which made it difficult to compare. The topology optimisation showed the upper end of the beam could be wider to more efficiently use material in future iterations, however the targets and objectives optimisation could have been refined more to achieve a better result.

7 References

ANSYS. (2021a). *ANSYS Workbench 2021 R1*.

ANSYS. (2021b). *Granta Edupack 2021 R2*. Ansys Inc.

Baccouch, M. (2021). A Brief Summary of the Finite Element Method for Differential Equations. In M. Baccouch (Ed.), *Finite Element Methods and Their Applications* (p. Ch. 1). IntechOpen. https://doi.org/10.5772/intechopen.95423

Dlubal Software. (2017, October 12). *Bimetallic Strip | Dlubal Software*. https://www.dlubal.com/en/downloads-and-information/examples-and-tutorials/verification-examples/000078

Goldberg, D. (1991). *What Every Computer Scientist Should Know About Floating-Point Arithmetic*.

Hearn, E. J. (1997). *Mechanics of Materials 2 : The Mechanics of Elastic and Plastic Deformation of Solids and Structural Materials: Vol. 3rd ed*. Butterworth-Heinemann. https://ezproxy.uwtsd.ac.uk/login?url=https://search.ebscohost.com/login.aspx?direct=true&db=nlebk&AN=199313&site=ehost-live

Hidalgo, R., Esnaola, J. A., Larrañaga, M., Llavori, I., Herrero-Dorca, N., Hurtado, I., Otxoa, E., Rodríguez, P., & Kortabarria, A. (2018). *Influence of Surface Finish and Porosity on the Fatigue behaviour of A356 Aluminium Casting Alloy*. https://doi.org/10.1051/matecconf/201816514007

Noble, A. (n.d.). *Piston Thermal Study Data*.

Rugarli, P., & Rugarli, P. (2010). *Structural analysis with finite elements* (1. publ). Telford.

Shenoy, P. S., & Fatemi, A. (2006). Dynamic analysis of loads and stress in connecting rods. *Proceedings of the Institution of Mechanical Engineers, Part C: Journal of Mechanical Engineering Science*, *220*(5), 615–624. https://doi.org/10.1243/09544062JMES105

SOLIDWORKS 2023. (2023). D'assault Systemes.